



**HAL**  
open science

# Arrangement of Monofunctional Silane Molecules on Silica Surfaces: Influence of Alkyl Chain Length, Head-Group Charge, and Surface Coverage, from Molecular Dynamics Simulations, X-ray Photoelectron Spectroscopy, and Fourier Transform Infrared Spectroscopy

Solène Lecot, Antonin Lavigne, Zihua Yang, Thomas Gehin, Claude Botella, Vincent Jousseume, Yann Chevolot, Magali Phaner-Goutorbe, Christelle Yeromonahos

► **To cite this version:**

Solène Lecot, Antonin Lavigne, Zihua Yang, Thomas Gehin, Claude Botella, et al.. Arrangement of Monofunctional Silane Molecules on Silica Surfaces: Influence of Alkyl Chain Length, Head-Group Charge, and Surface Coverage, from Molecular Dynamics Simulations, X-ray Photoelectron Spectroscopy, and Fourier Transform Infrared Spectroscopy. *Journal of Physical Chemistry C*, 2020, 124 (37), pp.20125-20134. 10.1021/acs.jpcc.0c05349 . hal-03214427

**HAL Id: hal-03214427**

**<https://hal.science/hal-03214427>**

Submitted on 1 May 2021

**HAL** is a multi-disciplinary open access archive for the deposit and dissemination of scientific research documents, whether they are published or not. The documents may come from teaching and research institutions in France or abroad, or from public or private research centers.

L'archive ouverte pluridisciplinaire **HAL**, est destinée au dépôt et à la diffusion de documents scientifiques de niveau recherche, publiés ou non, émanant des établissements d'enseignement et de recherche français ou étrangers, des laboratoires publics ou privés.

## C: Surfaces, Interfaces, Porous Materials, and Catalysis

**Arrangement of Monofunctional Silane Molecules on Silica Surfaces: Influence of the Alkyl Chain Length, Head-Group Charge and Surface Coverage, from Molecular Dynamics Simulations, X-Ray Photoelectron Spectroscopy and Fourier Transform Infrared Spectroscopy Analysis.**

Solène Lecot, Antonin Lavigne, Zihua Yang, Thomas Géhin, Claude Botella, Vincent Jousseume, Yann Chevotot, Magali Phaner-Goutorbe, and Christelle Yeromonahos

*J. Phys. Chem. C*, **Just Accepted Manuscript** • DOI: 10.1021/acs.jpcc.0c05349 • Publication Date (Web): 21 Aug 2020

Downloaded from [pubs.acs.org](https://pubs.acs.org) on August 25, 2020

**Just Accepted**

“Just Accepted” manuscripts have been peer-reviewed and accepted for publication. They are posted online prior to technical editing, formatting for publication and author proofing. The American Chemical Society provides “Just Accepted” as a service to the research community to expedite the dissemination of scientific material as soon as possible after acceptance. “Just Accepted” manuscripts appear in full in PDF format accompanied by an HTML abstract. “Just Accepted” manuscripts have been fully peer reviewed, but should not be considered the official version of record. They are citable by the Digital Object Identifier (DOI®). “Just Accepted” is an optional service offered to authors. Therefore, the “Just Accepted” Web site may not include all articles that will be published in the journal. After a manuscript is technically edited and formatted, it will be removed from the “Just Accepted” Web site and published as an ASAP article. Note that technical editing may introduce minor changes to the manuscript text and/or graphics which could affect content, and all legal disclaimers and ethical guidelines that apply to the journal pertain. ACS cannot be held responsible for errors or consequences arising from the use of information contained in these “Just Accepted” manuscripts.

1  
2  
3  
4  
5  
6  
7 Arrangement of Monofunctional Silane Molecules  
8  
9  
10  
11 on Silica Surfaces: Influence of the Alkyl Chain  
12  
13  
14  
15 Length, Head-Group Charge and Surface Coverage,  
16  
17  
18  
19 from Molecular Dynamics Simulations, X-Ray  
20  
21  
22  
23 Photoelectron Spectroscopy and Fourier Transform  
24  
25  
26  
27 Infrared Spectroscopy Analysis.  
28  
29  
30  
31  
32

33 *Solène Lecot<sup>§</sup>, Antonin Lavigne<sup>§</sup>, Zihua Yang<sup>§</sup>, Thomas Géhin<sup>§</sup>, Claude Botella<sup>§</sup>, Vincent*  
34 *Jousseaume<sup>⊥</sup>, Yann Chevolot<sup>§</sup>, Magali Phaner-Goutorbe<sup>§</sup>, Christelle Yeromonahos<sup>§\*</sup>*  
35  
36  
37

38 <sup>§</sup> Université de Lyon, Institut des Nanotechnologies de Lyon UMR 5270, Ecole Centrale de  
39  
40  
41 Lyon, 36 avenue Guy de Collongue, 69134 Ecully, France  
42  
43

44 <sup>⊥</sup> Université Grenoble Alpes, CEA, LETI, F-38000 Grenoble, France  
45  
46  
47  
48  
49  
50  
51

52 **\* Corresponding Author**  
53

54 Christelle Yeromonahos: christelle.yeromonahos@ec-lyon.fr, + 33 4 72 18 62 35  
55  
56  
57  
58  
59  
60

1  
2  
3 ABSTRACT  
4  
5  
6

7 Surface chemical functionalization is used in analytical tools to immobilize biomolecules that will  
8 capture a specific analyte, but also to reduce the nonspecific adsorption. Silane monolayers are  
9 widely used to functionalize silica surfaces. Their interfacial properties are linked to the silane  
10 organization. Here we study, by Molecular Dynamics simulations, the effects of silane molecule  
11 headgroup charge, alkyl chain length, and surface coverage on the structure of silane monolayers.  
12  
13 Four molecules are investigated: 3-aminopropyltrimethoxysilane, n-  
14 propyltrimethylmethoxysilane, octadecyltrimethylmethoxysilane, tert-butyl-11-  
15 (dimethylamino(dimethyl)silyl)undecanoate. The results suggest that, while long alkyl chains  
16 straighten out and adopt a more organized structure as surface coverage increases, the tilt angle of  
17 short chains is independent from surface coverage. Furthermore, in the case of long alkyl chains,  
18 a charged headgroup seems to reduce the tilt angle to surface coverage dependence. The simulated  
19 alkyl chain tilt angles were qualitatively validated by infrared spectroscopy and X-ray  
20 photoelectron spectroscopy. Also, a hexagonal packing is observed in all the monolayers, but is  
21 more defined as surface coverage increases. The nematic order parameter suggests that this  
22 packing is governed by the parallel orientation of the first C-C bonds near the surface. So, even  
23 short alkyl chains, with a large tilt angle distribution, present a hexagonal packing.  
24  
25  
26  
27  
28  
29  
30  
31  
32  
33  
34  
35  
36  
37  
38  
39  
40  
41  
42  
43  
44  
45  
46  
47  
48  
49  
50  
51  
52  
53  
54  
55  
56  
57  
58  
59  
60

## Introduction

A large number of applications takes advantage of surface chemical functionalization. In particular, in the field of biosensing, the specificity of the device (the fact of capturing solely a given analyte) and the signal to noise ratio are related to surface chemistry. For example, surface chemical functionalization allows the immobilization of biomolecules that will capture specifically biomarkers (peptides, proteins, DNA) or whole organisms for diagnosis purposes.<sup>1-6</sup> The background signal can also be reduced thanks to the chemical functionalization of material surfaces allowing the reduction of non-specific adsorption. Among the various chemical functionalizations, silane molecules have been widely used for the modification of oxides, especially oxidized silicon surfaces (SiO<sub>2</sub>).<sup>2,3,7-9</sup>

The structure, organization and surface energies of various silane modified SiO<sub>2</sub> surfaces have been studied by various characterization techniques as a function of experimental parameters, in particular in the case of multifunctional silane monolayers. Atomic Force Microscopy (AFM) experiments suggested that, after deposition on SiO<sub>2</sub> surface, silane molecules can diffuse laterally to self-assemble either into fractal network or into liquid phase state, depending on external parameters such as temperature.<sup>10</sup> Also, AFM studies have established that the strength of hydrophobic interactions on a silane monolayer is strongly related to the order of the silane molecules.<sup>11</sup> Indeed, pull-off forces resulting from hydrophobic adhesion are higher on crystalline-like monolayers than on liquid-like monolayers. The structure of *n*-alkane monolayers, with *n* > 12, has been extensively studied by Fourier Transform Infra-Red (FTIR) and X-Ray Diffraction (XRD) measurements.<sup>12-17</sup> While the positions of the methyl and methylene vibration modes from FTIR spectra yielded information on the presence of gauche defects in the alkyl chains and on the average alkyl chain tilt angle, the molecule crystalline packing inside the monolayer was addressed

1  
2  
3 by XRD measurements. Hexagonal crystalline-like domains with an intermolecular in-plane  
4 distance of 4.7-5 Å were observed for monolayers of *n*-alkylsilane molecules with  $n > 14$ .<sup>13,16</sup>  
5  
6 Shorter *n*-alkylsilane monolayers were shown to present more gauche defects than the longer ones,  
7  
8 but also a lower surface coverage.<sup>12</sup> Also, in the case of multifunctional silane molecules, a  
9  
10 Multiple Transmission and Reflection Infra-Red Spectroscopy study shown that the nature of the  
11  
12 leaving groups (Si(OMe)<sub>3</sub>, Si(OEt)<sub>3</sub>, Si(Cl)<sub>3</sub>) controls the rate of their hydrolysis, leading to very  
13  
14 different monolayer structures.<sup>17</sup>  
15  
16  
17  
18  
19

20 As the surface coverage cannot easily be varied experimentally, Molecular Dynamics (MD)  
21  
22 simulations are well suited to study the combined effects of surface coverage and alkyl chain length  
23  
24 of silane molecules on alkyl chain tilt angle, gauche defects and nematic order parameter.  
25  
26 However, only few MD simulations studies have addressed these questions. Different MD studies  
27  
28 suggested that the order parameter of *n*-alkylsilane monolayers (for  $n > 8$ ) increases as the alkyl  
29  
30 chain length and the surface coverage increase, while alkyl chain tilt angles are independent of  
31  
32 chain length and decrease as surface coverage increases.<sup>18-22</sup> Among them, it was also shown that  
33  
34 perfluorodecyltrichlorosilane (FDTS) monolayers at high surface coverage present a hexagonal  
35  
36 packing, whereas such packing was attenuated for octadecyltrichlorosilane (OTS) monolayers for  
37  
38 the same surface coverage.<sup>18</sup> In the present study, we demonstrate an effect of the head-group  
39  
40 charge and alkyl chain length ( $n < 18$ ), on the organization of the monolayer.  
41  
42  
43  
44  
45

46 We propose a MD simulation study on the effects of head-group charge (positive, neutral and  
47  
48 negative), alkyl chain length ( $n$  from 3 to 18), and surface coverage (1.5 to 4.2 nm<sup>-2</sup>) on the  
49  
50 structure of silane monolayers. The four different silane molecules are 3-  
51  
52 aminopropyldimethylethoxysilane (C<sub>7</sub>H<sub>19</sub>NOSi named NH<sub>3</sub><sup>+</sup>), n-propyldimethylmethoxysilane  
53  
54 (C<sub>6</sub>H<sub>16</sub>OSi named CH<sub>3</sub> short), octadecyldimethylmethoxysilane (C<sub>21</sub>H<sub>46</sub>OSi named CH<sub>3</sub> long), and  
55  
56  
57  
58  
59  
60

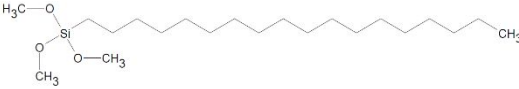
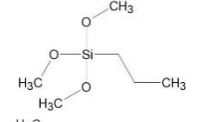
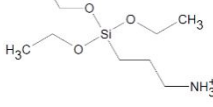
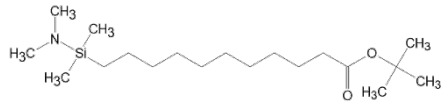
1  
2  
3 tert-butyl-11-(dimethylamino(dimethyl)silyl)undecanoate ( $C_{19}H_{41}NO_2Si$ , leading to  $COO^-$  after  
4 deprotection) (Table 1). The different silane monolayers were characterized by the alkyl chain tilt  
5 angle, the average number of gauche defects in the alkyl chains, the nematic order parameter for  
6 each C-C bond and its overall distribution, and the hexagonal packing of silane molecules on  $SiO_2$   
7 surface and its persistence length. To check that the simulated morphologies were consistent with  
8 experimental evidences, alkyl chain tilt angles were compared to experimental values obtained  
9 from FTIR-Attenuated Total Reflectance (FTIR-ATR) measurements. To this aim, four silane  
10 monolayers (one per silane molecule type) were elaborated from a liquid phase process on  $SiO_2$   
11 surfaces. The surface coverages were estimated by X-ray Photoelectron Spectroscopy (XPS)  
12 analysis.  
13  
14  
15  
16  
17  
18  
19  
20  
21  
22  
23  
24  
25  
26

## 27 **1. Materials and methods**

### 28 *1-1. Experimental materials and methods*

29  
30  
31  
32  
33 **Materials.**  $SiO_2$  (20 nm) / Aluminium (200 nm) / Silicon substrates were prepared by Physical  
34 Vapor Deposition (PVD) using a 200 mm Applied Materials Endura 5500 platform. The  
35 depositions were performed on Si (100) wafers without air break between Aluminium and  $SiO_2$ .  
36 3-aminopropyldimethylethoxysilane 95% ( $NH_3^+$ ), n-propyldimethylmethoxysilane 95% ( $CH_3$   
37 short) and octadecyldimethylmethoxysilane 95% ( $CH_3$  long) were purchased from ABCR. Tert-  
38 butyl-11-(dimethylamino(dimethyl)silyl)undecanoate (leading to  $COO^-$  after deprotection) was  
39 synthesized accordingly to a protocol previously reported.<sup>23</sup> The chemical structures of the four  
40 molecules are shown in Table 1.  
41  
42  
43  
44  
45  
46  
47  
48  
49  
50  
51  
52  
53  
54  
55  
56  
57  
58  
59  
60

**Table 1. The different silane molecules and surface coverage studied.**

Designation of silane molecule	Silane structural formula	Surface coverage used in MD simulations (nm <sup>-2</sup> )	Surface coverage estimated by XPS analysis (nm <sup>-2</sup> )
Systems with silane layer	CH <sub>3</sub> long 	1.5 – 3.0 – 4.2	3
	CH <sub>3</sub> short 	1.5 – 3.0 – 4.2	3
	NH <sub>3</sub> <sup>+</sup> 	3.0	8
	COO <sup>-</sup> 	3.0 – 4.2	3
System without silane layer	Bare SiO <sub>2</sub>		

**Chemical surface functionalization.** The substrates were cleaned by ozone/Ultraviolet treatment under oxygen flow for 30 min to remove organic contamination and to obtain a hydroxyl-terminated surface. Next, the substrates were heated at 150°C for 4 hours under nitrogen, allowed to cool to room temperature under nitrogen and then, the substrates were immersed in 10 ml dried pentane containing 90 µl of silane molecules. After 1 hour of incubation, the pentane was evaporated and the samples were heated at 150°C for 15 hours, to allow the silanization reaction. Finally, the samples were washed 10 minutes in tetrahydrofuran (THF) under sonication, and 10 minutes in ultrapure water under sonication.



1  
2  
3 **XPS analysis.** XPS measurements were performed using a VSW spectrometer equipped with a  
4 monochromatized X-ray source (Al K $\alpha$  1486.6 eV) in which the angle between the incident beam  
5 and the detector was the magic angle. The angular resolution was 3°. Take-off angle was 90°  
6 relative to the substrate surface. The energetic resolution was 0.2 eV. The data analysis was  
7 performed with CasaXPS software. Si(-O)<sub>4</sub> binding energy was set at 104 eV. A Shirley  
8 background was subtracted on Si2p and O1s spectra when coming from bulk elements while a  
9 linear background was subtracted on C1s spectra as surface elements. Peaks were fitted by a Gauss-  
10 Lorentz curve.  
11  
12  
13  
14  
15  
16  
17  
18  
19  
20  
21

22 **FTIR-ATR analysis.** FTIR-ATR was performed using a Thermo Nicolet 6700 spectrometer with  
23 a Mercury-Cadmium-Telluride (MCT) detector and a diamond crystal from 800 to 3000 cm<sup>-1</sup>.  
24 Results were obtained by averaging 256 scans with a resolution of 4 cm<sup>-1</sup>.  
25  
26  
27  
28  
29

### 30 *1-2. Computational methods*

31  
32  
33

34 **System description.** The silane molecules used are those presented in Table 1, after hydrolyzation,  
35 based on a trisilanol structure with two silanol groups remaining unreacted to behave similarly to  
36 a monofunctional silane (dimethylsilanol structure), as already reported in a previous study.<sup>24</sup> Such  
37 a structure was used because its force field is already known<sup>18</sup>, whereas the force field of  
38 dimethylsilanol is not published. The systems were built following the method proposed by  
39 Roscioni *et al.*<sup>18</sup> Silane molecules were initially randomly positioned on an amorphous SiO<sub>2</sub>  
40 surface, without explicit bonding between silane molecules and the surface, allowing their  
41 spontaneous lateral organization. As surface roughness has a strong influence on the lateral  
42 organization of silane molecules<sup>25</sup>, the parameters of amorphous SiO<sub>2</sub> surface published by  
43 Roscioni *et al.*<sup>18</sup> were used. Indeed, its Root Mean Square (RMS) value is close to the experimental  
44  
45  
46  
47  
48  
49  
50  
51  
52  
53  
54  
55  
56  
57  
58  
59  
60

1  
2  
3 value of SiO<sub>2</sub> thin films. Figure 1 illustrates the arrangement of the silane molecules on SiO<sub>2</sub>  
4 surface after 100-ns MD simulations. The simulation box included water molecules with the model  
5 TIP4P. The charges of the silane head-groups were compensated with counterions (Na<sup>+</sup> or Cl<sup>-</sup>) at  
6 a concentration of 150 mM to mimic physiological conditions. A Lennard-Jones (LJ) wall was  
7 added at the top of the box to avoid interactions between water and the bottom side of the SiO<sub>2</sub>  
8 surface and to prevent any surface curvature.<sup>26</sup> The simulation box included nearly 100 000 atoms  
9 and its dimensions are 7.8 nm x 7.8 nm x 15 nm.  
10  
11  
12  
13  
14  
15  
16  
17  
18  
19  
20  
21  
22  
23  
24  
25  
26  
27  
28  
29  
30  
31  
32  
33  
34  
35  
36  
37  
38  
39  
40  
41  
42  
43  
44  
45  
46  
47  
48  
49  
50  
51  
52  
53  
54  
55  
56  
57  
58  
59  
60

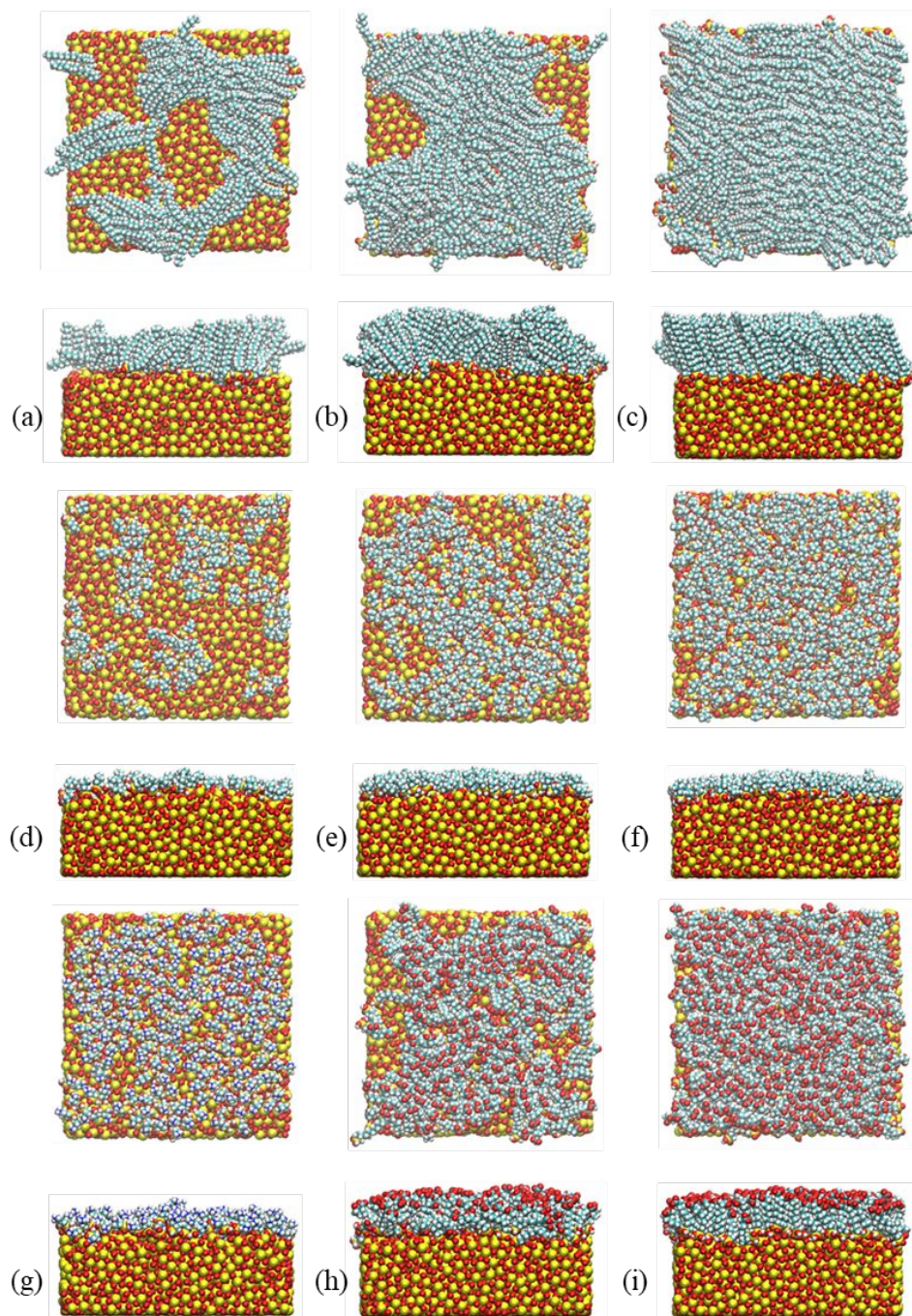


**Figure 1.** Arrangement of silane molecules on the amorphous  $\text{SiO}_2$  layer after 100 ns MD simulation for different silane head-groups, alkyl chain lengths and surface coverages : (a)  $\text{CH}_3$  long  $c = 1.5 \text{ nm}^{-2}$ , (b)  $\text{CH}_3$  long  $c = 3.0 \text{ nm}^{-2}$ , (c)  $\text{CH}_3$  long  $c = 4.2 \text{ nm}^{-2}$ , (d)  $\text{CH}_3$  short  $c = 1.5 \text{ nm}^{-2}$ , (e)  $\text{CH}_3$  short  $c = 3.0 \text{ nm}^{-2}$ , (f)  $\text{CH}_3$  short  $c = 4.2 \text{ nm}^{-2}$ , (g)  $\text{NH}_3^+$   $c = 3.0 \text{ nm}^{-2}$ , (h)  $\text{COO}^-$   $c = 3.0$

1  
2  
3 nm<sup>-2</sup> and (i) COO<sup>-</sup> c = 4.2 nm<sup>-2</sup>. Atoms are shown in yellow (silicon), red (oxygen), cyan  
4  
5 (carbon), white (hydrogen) and blue (nitrogen).  
6  
7

8  
9 **Simulation details.** All the simulations were performed with the Gromacs simulation package,  
10 version 5.1.3<sup>27</sup> and the VMD software package version 1.9.3<sup>28</sup> was used for visualization. Firstly,  
11 energy minimization was applied to the system using the Steepest Descent Minimization method.  
12 Then, NVT and NPT equilibrations were carried during 100 ps each, and production simulations  
13 were performed for 100 ns. A leap-frog algorithm was used for integration of the equations of  
14 motion with a time step of 2 fs. Constraints were applied to bond parameters with a LINCS  
15 algorithm. The temperature was maintained at 300 K with a Nose-Hoover thermostat using a time  
16 constant of 0.4 ps and the pressure was kept at 1 bar with a Parrinello-Rahman barostat using a  
17 time constant of 2 ps. Water and ions were both described with OPLS all-atom force-field.<sup>29</sup> The  
18 parameters to describe the LJ wall were taken from a previous study.<sup>26</sup> Force-field for both silane  
19 molecules and SiO<sub>2</sub> surfaces were adapted from recent studies<sup>18,19</sup>, and from the OPLS<sup>29</sup> all-atom  
20 force field. LJ potentials were truncated with a cut-off distance of 1 nm. Long range electrostatic  
21 interactions were calculated with the Particle Mesh Ewald method and a cut-off of 1 nm.  
22  
23  
24  
25  
26  
27  
28  
29  
30  
31  
32  
33  
34  
35  
36  
37  
38

39 **Analysis parameters.** The following parameters were evaluated by using Gromacs functions,  
40 VMD tools and home-made Python codes. The errors bars were estimated using the standard  
41 deviation. The curves and histograms were fitted using Bézier functions.  
42  
43  
44  
45  
46

47 *Tilt angles.* The alkyl chain tilt angle is defined as the angle  $\alpha$  between the normal to the SiO<sub>2</sub>  
48 surface and the vector between the silicon and terminal atoms of the silane molecule.<sup>18</sup>  
49  
50  
51  
52

53 *Gauche defects.* Gauche defect parameter was evaluated as the proportion of C-C-C-C torsion  
54 angles in *trans* conformation.<sup>30</sup> For each silane molecule, we calculated all its C-C-C-C torsion  
55  
56  
57  
58  
59  
60

1  
2  
3 angle  $\phi$ . If  $150^\circ \leq \phi \leq 180^\circ$ , the angle is in *trans* conformation and if  $50^\circ \leq \phi \leq 150^\circ$ , the angle is  
4  
5 in *gauche* conformation. Gauche defect parameter is the ratio  $r_{\text{trans}}$  between the number of *trans*  
6  
7 conformations and the total of *trans* and *gauche* conformations.  
8  
9

10  
11 *Nematic order parameter.* The chemical bond order parameter  $S_2^i$  describes the orientation of the  
12  
13  $i^{\text{th}}$  chemical bond, in a silane molecule, relative to the surface normal.<sup>30</sup> It is defined as:  
14  
15

$$16 \quad S_2^i = \frac{3 \cos^2 \varphi_i - 1}{2}$$

17  
18  
19  
20  
21 where  $\varphi_i$  is the angle between the  $i^{\text{th}}$  C-C bond and the surface normal.  $S_2^i$  takes values between -  
22  
23 0.5 and 1, where -0.5 corresponds to a bond parallel to the surface and 1 corresponds to a bond  
24  
25 perpendicular to the surface. We investigated the  $\langle S_2^i \rangle$  value (average on all the silane molecules  
26  
27 of  $S_2^i$  values for a given  $i^{\text{th}}$  bond) and the  $S_2$  distribution (probability of each  $S_2$  value independently  
28  
29 of the bond number in the alkyl chain). In a group of randomly oriented bonds,  $\langle S_2 \rangle = 0$  whereas  
30  
31  $\langle S_2^i \rangle = 0$  means that  $\langle \varphi_i \rangle = 55^\circ$ .  
32  
33  
34  
35  
36

37 *Radial Distribution Function (RDF).* The 2D radial distribution of silane molecules was  
38  
39 investigated in the  $(x,y)$  plane ( $\text{SiO}_2$  plane surface), taking into account periodic boundary  
40  
41 conditions. It is proportional to the probability of finding the Si atom of a silane neighboring  
42  
43 molecule for a given position on the plane, while the Si atom of the reference silane molecule is  
44  
45 fixed at origin.<sup>18,31</sup>  
46  
47  
48

## 49 **2. Results and Discussion**

### 50 *2.1 MD simulations*

Previous studies have shown the effects of alkyl chain length, with more than 6 carbon atoms ( $n > 6$ ), at different surface coverages, on the structural properties of silane monolayers. In this study, we decipher the impact of charged functional head-group and alkyl chain length, with more than 3 carbon atoms ( $n > 3$ ), at different surface coverages, on the structural properties of silane monolayers. MD simulations have been performed for all systems during 100 ns. The silane molecule diffusion distance is stabilized rapidly after 30 ns in all systems (Supporting information, Figure S1). After this diffusion phase, the Si atom of silane molecules can be considered as covalently fixed to the O atom of SiO<sub>2</sub>. The alkyl chain tilt angle  $\alpha$ , nematic order parameter  $\langle S_2 \rangle$  and gauche defect fraction  $r_{\text{trans}}$  are correlated to the crystal packing of silane molecules. The results are summarized in Table 2.

**Table 2. Alkyl chain tilt Angle, Nematic Order Parameter and Gauche Defect Parameter of the Silane Monolayers Studied.**

System	Alkyl chain tilt angle <sup>(a)</sup>		Nematic order parameter $\langle S_2 \rangle$		Gauche defect parameter	
	$\alpha$ (°)	FWHM <sup>(b)</sup> (°)	Even bond	Odd bond	$r_{\text{trans}}$	
CH <sub>3</sub> long	$c = 1.5 \text{ nm}^{-2}$	40	38	0.05	0.03	0.81
	$c = 3.0 \text{ nm}^{-2}$	34	26	0.06	0.22	0.85
	$c = 4.2 \text{ nm}^{-2}$	32	24	0.04	0.40	0.89
CH <sub>3</sub> short	$c = 1.5 \text{ nm}^{-2}$	22	53	-0.04	0.32	(c)
	$c = 3.0 \text{ nm}^{-2}$	22	35	-0.04	0.42	(c)
	$c = 4.2 \text{ nm}^{-2}$	22	32	-0.03	0.53	(c)
NH <sub>3</sub> <sup>+</sup>	$c = 3.0 \text{ nm}^{-2}$	23	57	0.17	0.05	(c)
COO <sup>-</sup>	$c = 3.0 \text{ nm}^{-2}$	19	27	0.20	0.16	0.69
	$c = 4.2 \text{ nm}^{-2}$	20	30	0.26	0.23	0.70

1  
2  
3 (a) Tilt angle distribution are depicted in Supporting Information, Figure S2. (b) Full Width at Half  
4 Maximum (FWHM). (c)  $r_{\text{trans}}$  value is not relevant for small molecules with only one torsion angle.  
5  
6  
7  
8  
9

10 **Tilt angle.** As shown in Table 2 (and Figure S2 in Supporting Information), the average tilt angle  
11 of CH<sub>3</sub> long molecules increases from 32° to 40°, while the Full Width at Half Maximum (FWHM)  
12 of the tilt angle distribution increases from 24° to 38°, as the surface coverage decreases from 4.2  
13 nm<sup>-2</sup> to 1.5 nm<sup>-2</sup>. This indicates that CH<sub>3</sub> long molecules straighten out and adopt a more organized  
14 structure, as the coverage increases. These results are in agreement with previous MD studies, for  
15 long alkyl chains ( $n > 8$ )<sup>18-20</sup>, and can be explained by an increase in Van der Waals forces between  
16 alkyl chains as their amount increases. However, very short alkyl chains (CH<sub>3</sub> short, NH<sub>3</sub><sup>+</sup>,  $n = 3$ )  
17 seem to behave very differently from long ones ( $n > 8$ ). The average tilt angles of NH<sub>3</sub><sup>+</sup> and CH<sub>3</sub>  
18 short molecules seem to be independent of the studied surface coverages and they are similar,  
19 around 20°. Furthermore, a charged head-group seems also to influence the tilt angle to surface  
20 coverage relationship of silane molecules with long alkyl chains ( $n > 8$ ). Indeed, despite a chain  
21 length of eleven carbon atoms ( $n = 11$ ), no influence of surface coverage was observed on the tilt  
22 angle of COO<sup>-</sup> silane molecules. Regarding on NH<sub>3</sub><sup>+</sup> and COO<sup>-</sup> molecules, repulsion between their  
23 charged functional head-groups can explain the widening in their tilt angles distribution. The tilt  
24 angle distribution of CH<sub>3</sub> short is larger than for CH<sub>3</sub> long, and the tilt angle distribution of NH<sub>3</sub><sup>+</sup>  
25 is larger than for COO<sup>-</sup> at a given surface coverage. It can be explained by the effect of Van der  
26 Waals forces between long alkyl chains. These results suggest that the FWHM of tilt angle  
27 distributions increases with charged head-groups and decreases as chain length increases.  
28  
29  
30  
31  
32  
33  
34  
35  
36  
37  
38  
39  
40  
41  
42  
43  
44  
45  
46  
47  
48  
49

50  
51 Moreover, the degree of aggregation of silane molecules (observed on Figure 1), can be related to  
52 the FWHM of the tilt angle distribution. Indeed, for a same coverage (*e.g.*  $c = 3.0 \text{ nm}^{-2}$ ), CH<sub>3</sub> long  
53  
54  
55  
56  
57  
58  
59  
60

1  
2  
3 molecules are positioned within a single and dense aggregate, CH<sub>3</sub> short molecules form several  
4 smaller aggregates separated by small non-functionalized SiO<sub>2</sub> areas, and silane molecules with  
5 charged head-groups seem more evenly dispersed on the surface. So, both charged head-groups  
6 and short alkyl chains seem to decrease silane molecule aggregation on the SiO<sub>2</sub> surface, while  
7 increasing the FWHM of the tilt angle distributions. Indeed, the FWHM of the tilt angle is smaller  
8 for CH<sub>3</sub> long monolayer (26°) than for CH<sub>3</sub> short (35°) and NH<sub>3</sub><sup>+</sup> monolayers (57°) (Table 2).  
9  
10 Actually, silane molecules within a single dense aggregate could tend to behave similarly to  
11 increase Van der Waals interactions (leading to a low FWHM value), while more evenly dispersed  
12 silane molecules could be less impacted by the neighboring silane (leading to a high FWHM  
13 value). However, COO<sup>-</sup> and CH<sub>3</sub> long monolayers have similar FWHM (27° and 26° respectively),  
14 despite very different surface distributions. This result could be explained by a balance between  
15 the opposite effects of the charged head-group and of the long alkyl chain of COO<sup>-</sup> molecules.  
16  
17  
18  
19  
20  
21  
22  
23  
24  
25  
26  
27  
28  
29

30  
31 So, the FWHM of the tilt angle distribution of silane molecules seems to depend, in the same way  
32 as the degree of dispersion of silane molecules on SiO<sub>2</sub> surface, on the presence of charged head-  
33 groups and on the alkyl chain length.  
34  
35  
36  
37  
38

39 **Gauche defects.** As shown in Table 2, CH<sub>3</sub> long silane molecules at low surface coverage ( $c = 1.5$   
40  $\text{nm}^{-2}$ ) present a lower  $r_{\text{trans}}$ , (0.81), which means that there are more gauche defects, than at higher  
41 coverages ( $r_{\text{trans}} = 0.85$  and  $r_{\text{trans}} = 0.89$  for  $c = 3.0 \text{ nm}^{-2}$  and  $c = 4.2 \text{ nm}^{-2}$ , respectively). These  
42 findings are in good agreement with experimental reports found in the literature.<sup>22,32,33</sup> COO<sup>-</sup>  
43 molecules have more gauche defects than CH<sub>3</sub> long molecules for the same coverage ( $r_{\text{trans}} = 0.69$   
44 and  $r_{\text{trans}} = 0.7$  for  $c = 3.0 \text{ nm}^{-2}$  and  $c = 4.2 \text{ nm}^{-2}$ , respectively). The presence of charged head-  
45 groups results in an increase in gauche defects. As the alkyl chains of NH<sub>3</sub><sup>+</sup> and CH<sub>3</sub> short silane  
46  
47  
48  
49  
50  
51  
52  
53  
54  
55  
56  
57  
58  
59  
60



1  
2  
3 molecules contain only one torsion angle, the calculation of their gauche defect parameter is not  
4  
5 relevant.  
6

7  
8 **Nematic order parameter.** As discussed above, in our CH<sub>3</sub> long monolayers, alkyl chains tilt  
9 angles are in the range of 32° to 40°. As a consequence, for perfectly parallel CH<sub>3</sub> long molecules,  
10 such angles should lead to  $S_2$  values in the range of 0.98 to 1 for each odd bond and in the range  
11 of -0.24 to -0.4 for each even bond. As the CH<sub>3</sub> long surface coverage increases, the odd bond  
12  $\langle S_2^{2n+1} \rangle$  value increases from 0.03 to 0.4, as shown in Figure 2. Also, as shown in Figure 3, the  $S_2$   
13 probability distribution shows that two values for odd and even bonds (1 and -0.25) are more and  
14 more represented as surface coverage increases. These results reveal that an organization of the  
15 CH<sub>3</sub> long molecules in a herringbone structure appears as coverage increases, in agreement with  
16 previous studies.<sup>18,22,30</sup> Thus, long alkyl chains (without head-groups) and high surface coverage  
17 lead to a well-ordered state, allowing a preferred alkyl chain orientation with few gauche  
18 distortions. Regarding CH<sub>3</sub> short monolayers, alkyl chain tilt angles are around 22°. As a  
19 consequence, for perfectly parallel CH<sub>3</sub> short molecules, such angles should lead to a  $S_2$  value of  
20 0.94 for the odd bond. Our results show that the CH<sub>3</sub> short odd bond  $\langle S_2^1 \rangle$  value is 0.4 at  $c = 3.0$   
21 nm<sup>-2</sup> and 0.53 at  $c = 4.2$  nm<sup>-2</sup>, which is much higher than the odd bond  $\langle S_2^{2n+1} \rangle$  values of CH<sub>3</sub> long  
22 (respectively 0.2 and 0.4). Even if CH<sub>3</sub> short molecules have a large tilt angle distribution, the  
23 order parameter relative to their second C-C bond is high, meaning that this C-C bond seems highly  
24 ordered through the monolayer. In the case of NH<sub>3</sub><sup>+</sup> and COO<sup>-</sup> molecules,  $\langle S_2^i \rangle$  values are close to  
25 0 for even as well as for odd bonds, and the herringbone structure is not observed (Figure 2), even  
26 at high coverage for COO<sup>-</sup> molecules. All these observations suggest that the presence of charged  
27 head-groups results in a more disordered monolayer.  
28  
29  
30  
31  
32  
33  
34  
35  
36  
37  
38  
39  
40  
41  
42  
43  
44  
45  
46  
47  
48  
49  
50  
51  
52  
53  
54  
55  
56  
57  
58  
59  
60

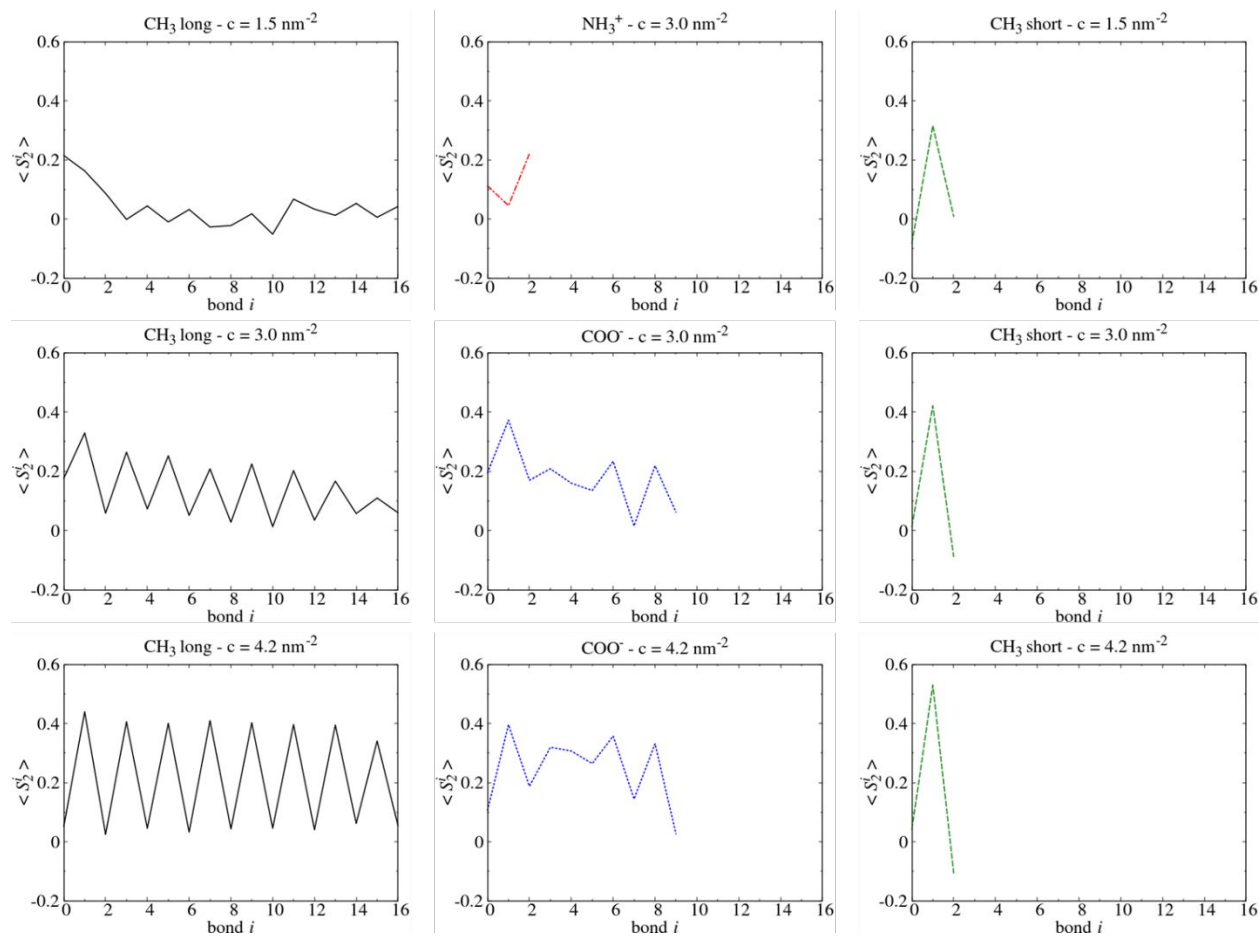
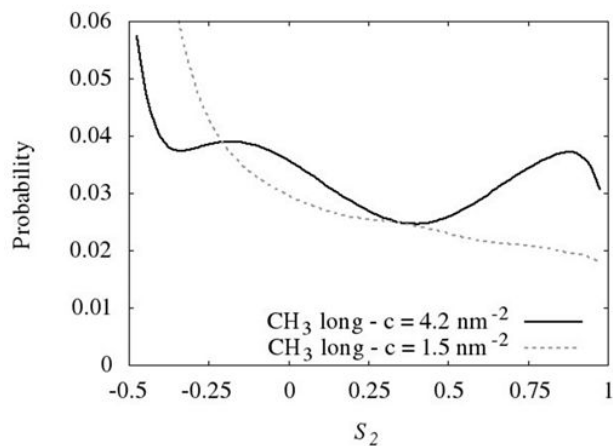


**Figure 2.** Average nematic order parameter  $\langle S_2^i \rangle$  computed for each C-C or C-N bond of the different silane monolayers. Silane molecules present a herringbone structure when  $\langle S_2^i \rangle$  varies periodically between odd and even bonds.



1  
2  
3 **Figure 3.** Distribution of the nematic order parameter  $S_2$  for  $\text{CH}_3$  long silane monolayer at  
4 surface coverage  $c = 1.5 \text{ nm}^{-2}$  and  $c = 4.2 \text{ nm}^{-2}$ .  $S_2 = 0$  corresponds to a bond parallel to the  
5 surface. For  $\text{CH}_3$  long ( $c = 4.2 \text{ nm}^{-2}$ ) values around -0.25 and 1 are more probable, which  
6  
7  
8  
9  
10 corresponds to the  $S_2$  values for a tilt angle of  $32^\circ$ .

11  
12  
13 **2D Radial Distribution Function.** The high nematic order parameters at high surface coverages  
14 for  $\text{CH}_3$  long suggest the presence of a positional order in these monolayers. To assess it, the two  
15 dimensional Radial Distribution Function (RDF) in the  $(x,y)$  plane was calculated.<sup>18,34</sup> At initial  
16 state, because the silane molecules are randomly positioned in the  $(x,y)$  plane, the RDF is a line  
17 whose slope is directly proportional to the surface coverage (Supporting Information, Figure S3).  
18 At final state, all the systems present several peaks, which means that positional order and  
19 periodicity appear even for the  $\text{NH}_3^+$  silane molecules (Figure 4). As shown in Figure 5, for  $\text{CH}_3$   
20 long silane monolayers at  $c = 3.0 \text{ nm}^{-2}$  and  $c = 4.2 \text{ nm}^{-2}$ , the 2D maps of the RDF clearly present a  
21 hexagonal packing. This means that each silane molecule has six closest neighbors, spaced by 0.5  
22 nm. For  $c = 1.5 \text{ nm}^{-2}$ , the hexagonal packing is less obvious and the intensity of the first peak  
23 decreases. It can be explained by defects (absence of molecules at some places) in the monolayer  
24 due to low surface coverage, as shown in Figure 1. These results are in agreement with previous  
25 MD studies.<sup>18,34</sup>

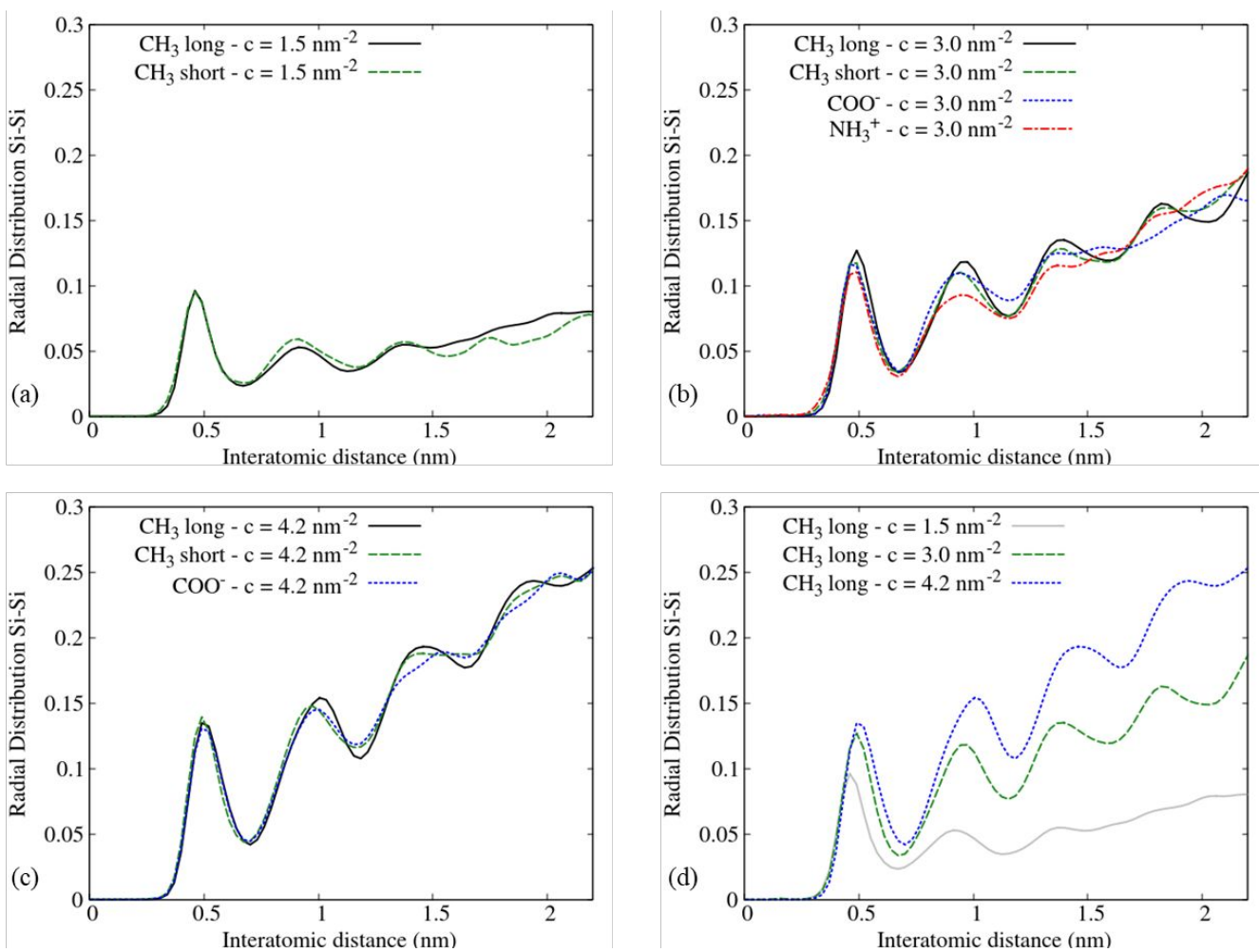


**Figure 4.** Radial distribution functions (RDF) of silane monolayers at different surface coverages: (a)  $c = 1.5 \text{ nm}^{-2}$ , (b)  $c = 3.0 \text{ nm}^{-2}$ , (c)  $c = 4.2 \text{ nm}^{-2}$  and (d)  $\text{CH}_3$  long at different coverages after 100 ns MD simulation. The peaks observed at a periodic interatomic distance show that a positional order appears in the silane monolayers.

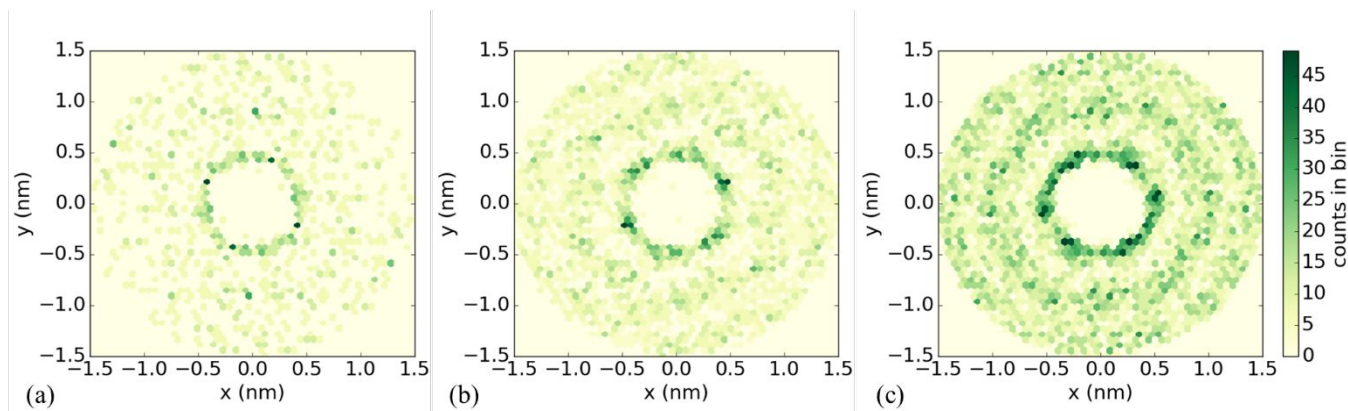


**Figure 5.** Two-dimensional Si – Si radial distribution functions of CH<sub>3</sub> long silane monolayer at different surface coverages (arbitrary units): (a)  $c = 1.5 \text{ nm}^{-2}$ , (b)  $c = 3.0 \text{ nm}^{-2}$  and (c)  $c = 4.2 \text{ nm}^{-2}$ . A hexagonal positional order appears when surface coverage of alkylsilane molecules increases.

Moreover, our results show that, whatever the monolayer studied, independently of alkyl chain length and head-group charge, the first peak (*i.e.* lattice parameter, minimum Si-Si distance between two neighboring molecules) is shifted towards higher values as surface coverage increases, reaching 0.45 nm at  $c = 1.5 \text{ nm}^{-2}$ , 0.49 nm at  $c = 3.0 \text{ nm}^{-2}$ , and 0.5 nm at  $c = 4.2 \text{ nm}^{-2}$ . This result can be explained by the flexibility of the alkyl chains. Indeed, their higher flexibility at low surface coverage could allow Si atoms from silane molecules to position themselves closer to each other, during the diffusion phase of the MD simulation, while respecting the Van der Waals radius of the Si atom (which is 0.21 nm). For a given surface coverage, the intensity of the first peak is the same whatever the system. It means that the number of closest neighbor silane molecules does not depend on alkyl chain length and on charged head-groups. For CH<sub>3</sub> short and CH<sub>3</sub> long molecules at  $c = 3.0 \text{ nm}^{-2}$  and  $c = 4.2 \text{ nm}^{-2}$ , the RDF shows that the hexagonal packing persists on the  $(x,y)$  plane, up to 2 nm around the origin as four peaks are well-defined on Figure 4. It is not the case for charged head-groups, only the two first peaks are visible meaning that the

1  
2  
3 propagation of the hexagonal packing is limited up to 1.5 nm. Consequently,  $\text{NH}_3^+$  and  $\text{COO}^-$   
4 silane monolayers are more disordered than  $\text{CH}_3$  short and  $\text{CH}_3$  long monolayers.  
5  
6

7  
8 To conclude, the persistence length of the hexagonal packing can be correlated with the nematic  
9 order parameter, as it increases with surface coverage, it is independent of chain length and tilt  
10 angle distribution, and it is prevented by charged head-groups. Thus, among the four investigated  
11 silane monolayers, it seems that  $\text{CH}_3$  long and  $\text{CH}_3$  short monolayers at coverages  $c = 3 \text{ nm}^{-2}$  and  
12  $c = 4.2 \text{ nm}^{-2}$ , lead to the highest positional order. However,  $\text{CH}_3$  short silane molecules have a  
13 larger tilt angle distribution than  $\text{CH}_3$  long silane molecules. Also, the persistence length of the  
14 hexagonal packing seems to be related to the degree of aggregation on the surface observed on  
15 Figure 1. Indeed, for a coverage of  $3.0 \text{ nm}^{-2}$ , four peaks are well-defined on the RDF plots for  $\text{CH}_3$   
16 long and  $\text{CH}_3$  short monolayers, while only two peaks are well-defined for  $\text{NH}_3^+$  and  $\text{COO}^-$   
17 monolayers (Figure 4b). This result suggests that the persistence length of the hexagonal packing  
18 increases with the degree of aggregation of silane molecules.  
19  
20  
21  
22  
23  
24  
25  
26  
27  
28  
29  
30  
31  
32

### 33 34 35 *2.2. Experimental validation of the simulated morphology*

36  
37 Previous experimental studies have shown that molecules with long alkyl chains are more ordered,  
38 they present smaller tilt angles, and are more densely packed on surface than molecules with short  
39 alkyl chains.<sup>11,12,35-37</sup> Most of the experimental studies are focused on multifunctional silane  
40 molecules, allowing silane cross-linking, whereas in the MD simulations monofunctional silane  
41 molecules are used. The monolayer morphology depends on the nature of silane molecules.<sup>36</sup> So,  
42 to check that our simulation results are consistent with experiments, FTIR-ATR analysis were  
43 carried out to qualitatively compare the alkyl chain tilt angle of the  $\text{NH}_3^+$ ,  $\text{COO}^-$ ,  $\text{CH}_3$  short and  
44  $\text{CH}_3$  long monolayers. The surface coverages were estimated by XPS measurements.  
45  
46  
47  
48  
49  
50  
51  
52  
53  
54  
55  
56  
57  
58  
59  
60

**XPS analysis.** XPS survey spectra of the bare SiO<sub>2</sub>/Aluminium/Silicon substrate, and of the four silanized SiO<sub>2</sub>/Aluminium/Silicon substrates are shown on Figures S4 - S8 (Supporting Information). The bare substrate shows distinct O1s and Si2p peaks, while C1s is not detected. Silanized substrates show distinct C1s, O1s and Si2p peaks, their binding energies are reported in Table S1 (Supporting Information). C1s, O1s, and Si2p core levels are shown on Figure S5 – S8 (Supporting Information). Two contributions are present in the high resolution Si2p spectra for the silanized substrates, which are associated to Si(-O)<sub>4</sub> and to Si(-O)<sub>1</sub> (Table S1, Supporting Information). The Si(-O)<sub>4</sub> contribution is consistent with the silicon associated with oxygen in the silica substrate. The presence of Si(-O)<sub>1</sub> contribution comforts the success of the silanization. Indeed, the four silanes used in this study are monovalent. The atomic percentages of the bare substrate and of the four silanized substrates are reported in Table S1 (Supporting Information). The Si:O ratio is about 1.6 for each substrate. The Si(-O)<sub>4</sub>:C ratio is consistent with the silane molecular composition, except for CH<sub>3</sub> short monolayer. Indeed, carbon contamination appears systematically on CH<sub>3</sub> short monolayer, although the silane solution is not contaminated.

The surface coverage of silanes,  $\Gamma_{silanes}$ , is estimated from the formula:<sup>38</sup>

$$\Gamma_{silanes} = \frac{A_{Si(-O)_1}}{A_{Si2p}} n_{SiO_2} z$$

where  $A_{Si(-O)_1}$  and  $A_{Si2p}$  are the normalized area of the Si(-O)<sub>1</sub> peak and of (Si(-O)<sub>1</sub> + Si(-O)<sub>4</sub>) components respectively,  $n_{SiO_2}$  is the molecular concentration of silica (22 nm<sup>-3</sup>) and  $z$  is the sampling depth.  $z$  is approximated by  $3\lambda$ , with  $\lambda$  is the mean free path in silica, equal to 3.7 nm.<sup>39,40</sup> The surface coverages are about 3 nm<sup>-2</sup> for CH<sub>3</sub> short, CH<sub>3</sub> long, and COO<sup>-</sup> monolayers, and around 8 nm<sup>-2</sup> for NH<sub>3</sub><sup>+</sup>. So, contrary to previous results obtained for multifunctional silanes<sup>12</sup>, the

1  
2  
3 coverage does not depend on the alkyl chain length. The  $\text{NH}_3^+$  surface coverage is more than two  
4 times higher than the surface coverage obtained with the other silane molecules. It might be  
5 explained by the catalytic effect of amino groups during silanization process.<sup>41,42</sup> Also, it is worth  
6 to be noticed that, because of sampling depth and variations in alkyl chain length, the calculation  
7 underestimates the ratio between the surface coverage of short alkyl chains ( $\text{CH}_3$  short or  $\text{NH}_3^+$ )  
8 and long alkyl chains ( $\text{CH}_3$  long or  $\text{COO}^-$ ).  
9  
10  
11  
12  
13  
14  
15  
16

17 **FTIR-ATR analysis.** It is well-known that the methylene asymmetric stretching mode is shifted  
18 to the lower frequency region as the alkyl chain order increases.<sup>11,17,43,44</sup> Moreover, several studies  
19 combining infrared spectroscopy, ellipsometry and AFM show that an increase in the alkyl chain  
20 order, or a shift to lower frequency region, is associated with a decrease in the alkyl chain tilt  
21 angle.<sup>12, 44</sup>  
22  
23  
24  
25  
26  
27  
28  
29

30 The FTIR-ATR spectra of the  $\text{COO}^-$ ,  $\text{CH}_3$  long and  $\text{NH}_3^+$  monolayers, shown in Figure 6, are  
31 dominated by the methylene symmetric stretching mode ( $\text{d}^+$ , in the range  $2854 \text{ cm}^{-1}$  -  $2858 \text{ cm}^{-1}$ )  
32 and the methylene asymmetric stretching ( $\text{d}^-$ , in the range  $2924 \text{ cm}^{-1}$  -  $2928 \text{ cm}^{-1}$ ) mode. These  
33 modes are not observed on the  $\text{CH}_3$  short monolayer, likely because the  $\text{CH}_3$  short molecule has  
34 fewer methylene groups than the  $\text{CH}_3$  long and  $\text{COO}^-$  molecules. However, despite  $\text{NH}_3^+$  and  $\text{CH}_3$   
35 short molecules have the same number of methylene groups,  $\text{d}^+$  and  $\text{d}^-$  modes are observed on the  
36  $\text{NH}_3^+$  monolayer. It can be explained by the higher surface coverage obtained with  $\text{NH}_3^+$  molecules  
37 than with  $\text{CH}_3$  short molecules ( $8 \text{ nm}^{-2}$  vs.  $3 \text{ nm}^{-2}$ ). Our results show a shift to low frequencies, by  
38 up to  $4 \text{ cm}^{-1}$ , for  $\text{d}^-$  modes of  $\text{CH}_3$  long ( $2929 \text{ cm}^{-1}$ ),  $\text{NH}_3^+$  ( $2927 \text{ cm}^{-1}$ ), and  $\text{COO}^-$  ( $2925 \text{ cm}^{-1}$ )  
39 monolayers. Such a shift suggests a higher tilt angle for  $\text{CH}_3$  long than for  $\text{NH}_3^+$  and  $\text{COO}^-$   
40 monolayers.<sup>44</sup> These results are in agreement with our tilt angles obtained by MD simulation.  
41  
42  
43  
44  
45  
46  
47  
48  
49  
50  
51  
52  
53  
54  
55  
56  
57  
58  
59  
60



of  $\text{NH}_3^+$  molecules at a coverage of  $4.2 \text{ nm}^{-2}$  and the one of  $\text{COO}^-$  at a coverage of  $3.0 \text{ nm}^{-2}$  are close, around  $12^\circ$ - $19^\circ$  (Supporting Information, Figure S2).

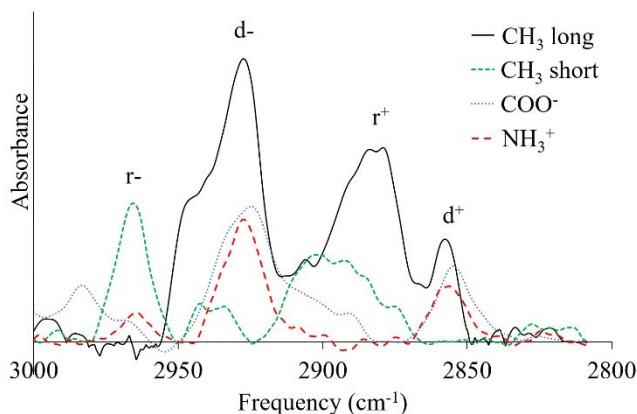


**Figure 6.** FTIR-ATR spectra of the four silanized surfaces.

The methyl asymmetric stretching mode ( $r^-$  in plane,  $2966 \text{ cm}^{-1}$ ) is clearly resolved on the  $\text{CH}_3$  short monolayer only, while the methyl symmetric stretching ( $r^+$ ,  $2878 \text{ cm}^{-1}$  and  $r^+$ FR  $2940 \text{ cm}^{-1}$ ) is clearly resolved on  $\text{CH}_3$  long monolayer, but not on  $\text{CH}_3$  short monolayer. Such results have already been observed from polarized FTIR-ATR experiments.<sup>12</sup> In polarized FTIR-ATR experiments, the  $r^-$  mode is observed only if the alkyl chains are nearly perpendicular to the surface, while the  $r^+$  mode is observed for alkyl chains with higher tilt angles only. In the present study, we cannot calculate the different tilt angles because we use an unpolarized FTIR-ATR equipment. However, our results suggest that a change in orientation occurs between  $\text{CH}_3$  long and  $\text{CH}_3$  short molecules. Indeed as surface coverage is the same for  $\text{CH}_3$  short and  $\text{CH}_3$  long monolayers, if there were no change in the average alkyl chain tilt angle, then the  $r^-$  and  $r^+$  peak areas of these two monolayers would be the same (with different widths, depending on the tilt angle distribution). By assuming that the presence of the  $r^-$  mode on the  $\text{CH}_3$  short system is not entirely linked to the carbon contamination, these experimental results are qualitatively in agreement with tilt angles

1  
2  
3 from our MD simulations, which suggest that the tilt angle of CH<sub>3</sub> long molecules is 34° while the  
4  
5 one of CH<sub>3</sub> short molecules is 22°.  
6  
7

8  
9 Previous experimental studies have shown that, in the case of multifunctional silane molecules,  
10  
11 the surface coverage increases, and the tilt angle decreases, as the alkyl chain length increases.<sup>12</sup>  
12  
13 Our experimental and simulated results suggest that, in the case of monofunctional silane  
14  
15 molecules, likely because of the absence of intermolecular bonds, the alkyl chain length has no  
16  
17 significant effect on the surface coverage. However, the average chain tilt angle increases as the  
18  
19 chain length increases.  
20  
21

### 22 23 **3. Conclusion** 24

25  
26 This study shows that the ordered state of the silane monolayer depends on the alkyl chain length  
27  
28 ( $n$  from 3 to 18), head-group charge, and on the surface coverage. Indeed, long alkyl chains and  
29  
30 high coverages lead to more organized self-assembled silane monolayers, with a narrow tilt angle  
31  
32 distribution centered on a preferred orientation, and few gauche distortions. Also, for given alkyl  
33  
34 chain length and surface coverage, charged silane molecules lead to a more disordered state than  
35  
36 neutral silane molecules, with a larger tilt angle distribution. Long alkyl chains ( $n > 8$ ) were  
37  
38 reported to have a tilt angle independent of chain length and to be affected by surface coverage.  
39  
40 On the contrary, short alkyl chains ( $n = 3$ ) behave very differently, since their tilt angle seems to  
41  
42 be independent from surface coverage. Furthermore, a charged head-group seems to influence the  
43  
44 tilt angle to surface coverage relationship of long alkyl chain ( $n > 8$ ). Indeed no influence of surface  
45  
46 coverage on the COO<sup>-</sup> ( $n = 11$ ) tilt angle was observed. The differences between the simulated tilt  
47  
48 angles, depending on the nature of silane molecules, are validated by FTIR-ATR analysis.  
49  
50  
51  
52  
53  
54  
55  
56  
57  
58  
59  
60

1  
2  
3 Moreover, our results suggest that a hexagonal packing is observed in all the studied silane  
4 monolayers. However, whatever the alkyl chain length, an increase in surface coverage lead to the  
5 more marked appearance of the hexagonal packing. Nematic order parameter values show that  
6 such packing is governed by the parallel orientation of the first C-C bonds of the silane molecules,  
7 near the SiO<sub>2</sub> surface. Thus, even short alkyl chain (CH<sub>3</sub> short), despite a large tilt angle  
8 distribution, present a well-defined hexagonal packing at high coverage.  
9

10  
11  
12 Surface chemical functionalization is used in analytical tools as a mean to immobilize  
13 biomolecules that will capture a specific analyte, but also to reduce the non-specific adsorption.  
14 This work could further help to understand the influence of the nature of silane molecules on the  
15 arrangement of the silane monolayer on SiO<sub>2</sub> surfaces, and on subsequent biomolecule  
16 interactions, to design more efficient analytical tools.  
17  
18  
19  
20  
21  
22  
23  
24  
25  
26  
27  
28  
29  
30  
31

## 32 ASSOCIATED CONTENT

33  
34  
35  
36 The following files are available free of charge.

37  
38  
39 Diffusion distance of silane molecules. Tilt angle distributions. Sub-coverages for each system  
40 studied at 3 nm<sup>-2</sup> and 1.5 nm<sup>-2</sup>. Radial distribution functions of CH<sub>3</sub> long silane molecules. XPS  
41 spectra. XPS binding energy and atomic percentages. (PDF)  
42  
43  
44  
45  
46

## 47 AUTHOR INFORMATION

### 48 49 50 **Corresponding Author**

51  
52  
53 \*Email: christelle.yeromonahos@ec-lyon.fr  
54  
55  
56  
57  
58  
59  
60

## Author Contributions

The manuscript was written through contributions of all authors. All authors have given approval to the final version of the manuscript.

## Funding Sources

This work was supported by the Young Researcher ANR PORIDG project, grant ANR-18-CE09-0006 of the French Agence Nationale de la Recherche. This work was granted access to the HPC resources of CINES under the allocation 2019-A0070711100 made by GENCI. Also, this work was supported by the PMCS2I - supercomputer Newton from Ecole Centrale de Lyon, France, member of the FLMSN.

## ACKNOWLEDGMENT

The authors thank Laurent Pouilloux, Anne Cadiou, and Laurent Carrel for support on PMCS2I resources.

## REFERENCES

- (1) Beaucage, S. L. Strategies in the preparation of DNA oligonucleotide arrays for diagnostic applications. *Curr. Med. Chem.* **2001**, *8*, 1213-1244.
- (2) Beier, M.; Hoheisel, J. D. Versatile derivatisation of solid support media for covalent bonding on DNA-microchips. *Nucleic Acids Res.* **1999**, *27*, 1970-1977.
- (3) Wang, Y.; Cai, J.; Rauscher, H.; Behm, R. J.; Goedel, W. A. Maleimido-Terminated Self-Assembled Monolayers. *Chem. Eur. J.* **2005**, *11*, 3968-3978.

- 1  
2  
3 (4) Luderer F.; Walschus U. Immobilization of Oligonucleotides for Biochemical Sensing by Self-  
4 Assembled Monolayers: Thiol-Organic Bonding on Gold and Silanization on Silica Surfaces.  
5  
6 Wittmann C. (eds) *Immobilisation of DNA on Chips I. Topics in Current Chemistry Springer,*  
7  
8 *Berlin Heidelberg* **2005**, 260, 37-56.  
9  
10  
11  
12  
13 (5) Hitaishi, V. P. ; Clement, R. ; Bourassin, N. ; Baaden, M. ; De Poulpiquet, A. ; Sacquin-Mora,  
14  
15 S. ; Ciaccafava, A. ; Lojou, E. Controlling redox enzyme orientation at planar electrodes. *Catalysts*  
16  
17 **2018**, 8, 192.  
18  
19  
20  
21 (6) Ruan, M.; Seydou, M.; Noel, V.; Piro, B.; Maurel, F.; Barbault, F. Molecular dynamics  
22  
23 simulation of a RNA aptasensor. *J. Phys. Chem. B* **2017**, 121, 4071-4080.  
24  
25  
26 (7) Chu-jiang, C.; Zhi-gang, S.; Yu-shan, X.; Shu-lin, M. Surface topography and character of  $\gamma$ -  
27  
28 aminopropyltriethoxysilane and dodecyltrimethoxysilane films adsorbed on the silicon dioxide  
29  
30 substrate via vapour phase deposition. *J. Phys. D: Appl. Phys.* **2006**, 39, 4829-4837.  
31  
32  
33  
34 (8) Halliwell, C. M.; Cass, A. E. A factorial analysis of silanization conditions for the  
35  
36 immobilization of oligonucleotides on glass surfaces. *Anal. Chem.* **2001**, 73, 2476-2483.  
37  
38  
39  
40 (9) Al-Hajj, N.; Mousli, Y.; Miche, A.; Humblot, V.; Hunel, J.; Heuzé, K.; Buffeteau, T.; Genin,  
41  
42 E.; Vellutini, L. Influence of the Grafting Process on the Orientation and the Reactivity of Azide-  
43  
44 Terminated Monolayers onto Silica Surface. *Appl. Surf. Sci.* **2020**, 146778.  
45  
46  
47 (10) Britt, D. W.; Hlady, V. An AFM study of the effects of silanization temperature, hydration,  
48  
49 and annealing on the nucleation and aggregation of condensed OTS domains on mica. *J. Colloid*  
50  
51 *Interface Sci.* **1996**, 178, 775-784.  
52  
53  
54  
55  
56  
57  
58  
59  
60

1  
2  
3 (11) Yeon, H.; Wang, C.; Van Lehn, R. C.; Abbott, N. L. Influence of Order within Nonpolar  
4 Monolayers on Hydrophobic Interactions. *Langmuir* **2017**, *33*, 4628-4637.

5  
6  
7  
8 (12) Barrett, A.; Petersen, P. B. Order of dry and wet mixed-length self-assembled monolayers. *J.*  
9 *Phys. Chem. C* **2015**, *119*, 23943-23950.

10  
11  
12 (13) Steinrück, H. G.; Will, J.; Magerl, A.; Ocko, B. M. Structure of n-Alkyltrichlorosilane  
13 Monolayers on Si (100)/SiO<sub>2</sub>. *Langmuir* **2015**, *31*, 11774-11780.

14  
15 (14) Wen, K.; Maoz, R.; Cohen, H.; Sagiv, J.; Gibaud, A.; Desert, A.; Ocko, B. M. Postassembly  
16 chemical modification of a highly ordered organosilane multilayer: New insights into the structure,  
17 bonding, and dynamics of self-assembling silane monolayers. *ACS nano* **2008**, *2*, 579-599.

18  
19 (15) Koga, T.; Honda, K.; Sasaki, S.; Sakata, O.; Takahara, A. Phase transition of alkylsilane  
20 monolayers studied by temperature-dependent grazing incidence X-ray diffraction. *Langmuir*  
21 **2007**, *23*, 8861-8865.

22  
23 (16) Ito, Y.; Virkar, A. A.; Mannsfeld, S.; Oh, J. H.; Toney, M.; Locklin, J.; Bao, Z. Crystalline  
24 ultrasmooth self-assembled monolayers of alkylsilanes for organic field-effect transistors. *J. Am.*  
25 *Chem. Soc.* **2009**, *131*, 9396-9404.

26  
27 (17) Naik V.V.; Städler R.; Spender N.D. Effect of leaving group on the structures of alkylsilane  
28 SAMs. *Langmuir* **2014**, *30*, 14824-14831.

29  
30 (18) Roscioni, O. M.; Muccioli, L.; Mityashin, A.; Cornil, J.; Zannoni, C. Structural  
31 characterization of alkylsilane and fluoroalkylsilane self-assembled monolayers on SiO<sub>2</sub> by  
32 molecular dynamics simulations. *J. Phys. Chem. C* **2016**, *120*, 14652-14662.

1  
2  
3 (19) Castillo, J. M.; Klos, M.; Jacobs, K.; Horsch, M.; Hasse, H. (2015). Characterization of  
4 alkylsilane self-assembled monolayers by molecular simulation. *Langmuir* **2015**, *31*, 2630-2638.  
5  
6

7  
8  
9 (20) Black, J. E.; Iacovella, C. R.; Cummings, P. T.; McCabe, C. Molecular dynamics study of  
10 alkylsilane monolayers on realistic amorphous silica surfaces. *Langmuir* **2015**, *31*, 3086-3093.  
11  
12

13  
14 (21) Black, J. E.; Summers, A. Z.; Iacovella, C. R.; Cummings, P. T.; McCabe, C. Investigation  
15 of the Impact of Cross-Polymerization on the Structural and Frictional Properties of Alkylsilane  
16 Monolayers Using Molecular Simulation. *Nanomaterials* **2019**, *9*, 639.  
17  
18

19  
20 (22) Ewers, B.W.; Batteas, J.D. Molecular dynamics simulations of alkylsilane monolayers on  
21 silica nanoasperities: impact of surface curvature on monolayer structure and pathways for energy  
22 dissipation in tribological contacts. *J. Phys. Chem. C* **2012**, *116*, 25165-25177.  
23  
24  
25  
26

27  
28 (23) Dugas, V.; Depret, G.; Chevalier, Y.; Nesme, X.; Souteyrand, É. Immobilization of single-  
29 stranded DNA fragments to solid surfaces and their repeatable specific hybridization: covalent  
30 binding or adsorption? *Sens. Actuator B-Chem.* **2004**, *101*, 112-121.  
31  
32  
33  
34

35  
36 (24) Lecot S.; Chevolut Y.; Phaner-Goutorbe M.; Yeromonahos C. Impact of silane monolayers  
37 on the adsorption of streptavidin on silica and its subsequent interactions with biotin: molecular  
38 dynamics and steered molecular dynamics simulations. *J. Phys. Chem. B* **2020**, *124*, 6786-6796.  
39  
40  
41  
42

43  
44 (25) Roscioni, O. M.; Muccioli, L.; Della Valle, R. G.; Pizzirusso, A.; Ricci, M.; Zannoni, C.  
45 Predicting the anchoring of liquid crystals at a solid surface: 5-cyanobiphenyl on cristobalite and  
46 glassy silica surfaces of increasing roughness. *Langmuir* **2013**, *29*, 8950-8958.  
47  
48  
49  
50

51  
52 (26) Kitabata, M.; Taddese, T.; Okazaki, S. Molecular dynamics study on wettability of poly  
53 (vinylidene fluoride) crystalline and amorphous surfaces. *Langmuir* **2018**, *34*, 12214-12223.  
54  
55  
56  
57

1  
2  
3 (27) Van Der Spoel, D.; Lindahl, E.; Hess, B., Groenhof, G.; Mark, A. E.; Berendsen, H. J.  
4 GROMACS: fast, flexible, and free. *J. Comput. Chem.* **2005**, *26*, 1701-1718.  
5  
6

7  
8 (28) Humphrey, W.; Dalke, A.; Schulten, K. VMD: visual molecular dynamics. *J. Mol. Graph.*  
9 **1996**, *14*, 33-38.  
10  
11

12  
13 (29) Jorgensen, W. L.; Maxwell, D. S.; Tirado-Rives, J. Development and testing of the OPLS all-  
14 atom force field on conformational energetics and properties of organic liquids. *J. Am. Chem. Soc.*  
15 **1996**, *118*, 11225-11236.  
16  
17  
18

19  
20 (30) Schulze, E.; Stein, M. Simulation of Mixed Self-Assembled Monolayers on Gold: Effect of  
21 Terminal Alkyl Anchor Chain and Monolayer Composition. *J. Phys. Chem. B* **2018**, *122*, 7699-  
22 7710.  
23  
24  
25  
26  
27

28  
29 (31) Anvari, M. H.; Liu, Q.; Xu, Z.; Choi, P. Molecular Dynamics Study of Hydrophilic Sphalerite  
30 (110) Surface as Modified by Normal and Branched Butylthiols. *Langmuir* **2018**, *34*, 3363-3373.  
31  
32  
33

34  
35 (32) Parikh, A. N.; Allara, D. L.; Azouz, I. B.; Rondelez, F. An intrinsic relationship between  
36 molecular structure in self-assembled n-alkylsiloxane monolayers and deposition temperature. *The*  
37 *J. Phys. Chem.* **1994**, *98*, 7577-7590.  
38  
39  
40  
41

42  
43 (33) Allara, D. L.; Nuzzo, R. G. Spontaneously organized molecular assemblies. 2. Quantitative  
44 infrared spectroscopic determination of equilibrium structures of solution-adsorbed n-alkanoic  
45 acids on an oxidized aluminum surface. *Langmuir* **1985**, *1*, 52-66.  
46  
47  
48  
49

50  
51 (34) Deetz, J. D.; Ngo, Q.; Faller, R. Reactive Molecular Dynamics Simulations of the Silanization  
52 of Silica Substrates by Methoxysilanes and Hydroxysilanes. *Langmuir* **2016**, *32*, 7045-7055.  
53  
54  
55  
56  
57  
58  
59  
60



- 1  
2  
3 (35) Porter, M. D.; Bright, T. B.; Allara, D. L.; Chidsey, C. E. Spontaneously organized molecular  
4 assemblies. 4. Structural characterization of n-alkyl thiol monolayers on gold by optical  
5 ellipsometry, infrared spectroscopy, and electrochemistry. *J. Am. Chem. Soc.* **1987**, *109*, 3559-  
6 3568.  
7  
8  
9  
10  
11  
12  
13 (36) Ulman, A. Formation and structure of self-assembled monolayers. *Chem. Rev.* **1996**, *96*,  
14 1533-1554.  
15  
16  
17  
18 (37) Pujari, S. P.; Scheres, L.; Marcelis, A. T. ; Zuilhof, H. Covalent surface modification of oxide  
19 surfaces. *Angew. Chem. Int. Ed.* **2014**, *53*, 6322-6356.  
20  
21  
22  
23  
24 (38) Shircliff, R. A.; Martin, I. T.; Pankow, J. W.; Fennell, J.; Stradins, P.; Ghirardi, M. L.; Cowley,  
25 S. W.; Branz, H. M. High-resolution X-ray photoelectron spectroscopy of mixed silane monolayers  
26 for DNA attachment. *ACS Appl. Mater. Interfaces* **2011**, *3*, 3285-3292.  
27  
28  
29  
30  
31 (39) Vickerman, J. C.; Gilmore, I. S. (Eds.) Surface analysis: the principal techniques. *John Wiley*  
32 *& Sons.* **2011**.  
33  
34  
35  
36  
37 (40) Tanuma, S.; Powell, C. J.; Penn, D. R. Calculations of electron inelastic mean free paths  
38 (IMFPS). IV. Evaluation of calculated IMFPS and of the predictive IMFPS formula TPP-2 for  
39 electron energies between 50 and 2000 eV. *Surf. Interface Anal.* **1993**, *20*, 77-89.  
40  
41  
42  
43  
44 (41) Kinkel, J. N.; Unger, K. K. Role of solvent and base in the silanization reaction of silicas for  
45 reversed-phase high-performance liquid chromatography. *J. Chromatogr. A*, **1984**, *316*, 193-200.  
46  
47  
48  
49  
50 (42) Fadeev, A. Y.; McCarthy, T. J. Self-assembly is not the only reaction possible between  
51 alkyltrichlorosilanes and surfaces: monomolecular and oligomeric covalently attached layers of  
52 dichloro- and trichloroalkylsilanes on silicon. *Langmuir* **2000**, *16*, 7268-7274.  
53  
54  
55  
56  
57  
58  
59  
60

(43) Ardès-Guisot, N.; Durand, J. O.; Granier, M.; Perzyna, A.; Coffinier, Y.; Grandidier, B.; Wallart X.; Stievenard, D. Trichlorosilane isocyanate as coupling agent for mild conditions functionalization of silica-coated surfaces. *Langmuir* **2005**, *21*, 9406-9408.

(44) Nam, H.; Granier, M.; Boury, B.; Park, S.Y. Functional organotrimethoxysilane derivative with strong intermolecular  $\pi-\pi$  interaction: One-pot grafting reaction on oxidized silicon substrates. *Langmuir* **2006**, *22*, 7132-7134.

For Table of Contents Only

